

# Lawrence Berkeley National Laboratory

## LBL Publications

### Title

Giant self-driven exciton-Floquet signatures in time-resolved photoemission spectroscopy of MoS<sub>2</sub> from time-dependent GW approach.

### Permalink

<https://escholarship.org/uc/item/03d9x82h>

### Journal

Proceedings of the National Academy of Sciences of USA, 120(32)

### Authors

Chan, Y-H

Qiu, Diana

da Jornada, Felipe

et al.

### Publication Date

2023-08-08

### DOI

10.1073/pnas.2301957120

Peer reviewed



# Giant self-driven exciton-Floquet signatures in time-resolved photoemission spectroscopy of MoS<sub>2</sub> from time-dependent GW approach

Y.-H. Chan<sup>a,b,c,d,1</sup> , Diana Y. Qiu<sup>a,b,e,1</sup> , Felipe H. da Jornada<sup>a,b,f,g,1</sup> , and Steven G. Louie<sup>a,b,1</sup>

Edited by Angel Rubio, Max-Planck-Institut für Struktur und Dynamik der Materie, Hamburg, Germany; received February 3, 2023; accepted June 13, 2023

Time-resolved, angle-resolved photoemission spectroscopy (TR-ARPES) is a one-particle spectroscopic technique that can probe excitons (two-particle excitations) in momentum space. We present an *ab initio*, time-domain GW approach to TR-ARPES and apply it to monolayer MoS<sub>2</sub>. We show that photoexcited excitons may be measured and quantified as satellite bands and lead to the renormalization of the quasiparticle bands. These features are explained in terms of an exciton-Floquet phenomenon induced by an exciton time-dependent bosonic field, which are orders of magnitude stronger than those of laser field-induced Floquet bands in low-dimensional semiconductors. Our findings imply a way to engineer Floquet matter through the coherent oscillation of excitons and open the new door for mechanisms for band structure engineering.

exciton | TR-ARPES | Floquet

Correlated electron-hole pair excitations, or excitons, typically dominate optical responses in semiconductors (1, 2), both in terms of optical strength and new features in the spectrum going beyond the independent-particle picture especially in reduced-dimensional systems. These correlated two-particle excitations are important in many optoelectronic applications (3) and lead to exotic phenomena such as exciton condensates (4–6) and singlet fission of excitons (7). Excitons are most often studied by optical experiments, in which optically active low-energy excitons can be identified as discrete energy states in the band gap. Further characterization of excitons may be obtained by how these states respond to external parameters such as temperature, carrier doping, strain, and additional external fields (8). In particular, pump-probe type optical experiments are able to provide essential information about how different exciton states couple (9, 10). In such experiments, a pump light is used to dress selected states and a probe light can then be used to detect the energy level shifts of the dressed exciton states. A careful theoretical analysis is necessary in general to provide the characterization.

Time-resolved, angle-resolved photoemission spectroscopy (TR-ARPES) is a well-established tool for studying the dynamics of electron response. The resolution of events on a femtosecond or attosecond scale allows for the investigation of nonequilibrium phenomena (11, 12), such as melting of phases (13, 14), ultrafast band gap renormalization (15, 16), and transient carrier dynamics (17–21). In recent years, the idea of using TR-ARPES to study excitons was proposed (22–25) and, more recently, realized experimentally (26–30). These TR-ARPES experiments have been able to attain the necessary low temperature, spot size, and momentum resolution to measure some expected spectroscopic signatures of excitons qualitatively: satellite features with a dispersion relation that follows a replica dispersion of the valence band, which are present even at times significantly after the passing of the external driving pump field (26, 27).

Several studies have addressed the possibility of visualizing exciton features in TR-ARPES theoretically using model Hamiltonians (22–25, 31). Quasi-equilibrium theory has also been applied to model a mixture of free carrier and bound excitons, where the spectral function shows a satellite structure due to excitons (32–35). In these quasi-equilibrium models (32–34), excitons or carriers are assumed to be in equilibrium (taking advantage of the time-scale difference between electron-electron scattering and electron scattering due to other degree of freedoms), and hence cannot address the fast electron dynamics in the femtosecond time scale. Recently, time-dependent simulations of model systems suggest interesting features in nonequilibrium samples, such as signatures of excitonic insulator-like features (34, 36). However, a time-dependent first-principles simulation of TR-ARPES for real materials that includes electron-hole interactions remains a major challenge and is currently under active development (37, 38).

## Significance

Engineering material properties through coherent optical fields has led to the discovery of light-induced transient superconductivity, ferroelectric transitions, and other exotic phases, which were previously thought to exist only in equilibrium. Here, we show that materials' electronic structure can also be engineered with a "self-driven exciton-Floquet effect," where the pump light creates excitons with a coherent polarization that itself acts as a driving field, independent of the light field. We demonstrate such effects in monolayer MoS<sub>2</sub> from first-principles calculations and show that it can provide an understanding to modify the material's band structure in time-resolved angle-resolved photoemission experiments.

Preprint Servers: <https://arxiv.org/abs/2302.01719>.

Author contributions: D.Y.Q., F.H.J., and S.G.L. designed research; Y.H.C. performed the calculations. All authors contributed to conceiving the research, analyzing the data, and writing the paper.

The authors declare no competing interest.

This article is a PNAS Direct Submission.

Copyright © 2023 the Author(s). Published by PNAS. This open access article is distributed under [Creative Commons Attribution-NonCommercial-NoDerivatives License 4.0 \(CC BY-NC-ND\)](https://creativecommons.org/licenses/by-nc-nd/4.0/).

<sup>1</sup>To whom correspondence may be addressed. Email: yanghao@gate.sinica.edu.tw, diana.qiu@yale.edu, jornada@stanford.edu, or sglouie@berkeley.edu.

This article contains supporting information online at <https://www.pnas.org/lookup/suppl/doi:10.1073/pnas.2301957120/-/DCSupplemental>.

Published July 31, 2023.

Here, we develop a first-principles GW approach in the time domain (39, 40) to compute the TR-ARPES in a pump-probe setup and apply it to the specific case of a monolayer MoS<sub>2</sub>. We show that the detailed properties of the optically bright excitons may be obtained, resulting from a modification of the spectral function (i.e., changes in the self-energy) of the measured hole, owing to the formation of excitons by the pump light. Additional features in the TR-ARPES occur as satellite bands at energies of the valence band plus an exciton excitation energy, and the **k**-dependent intensity of such satellite bands is proportional to the exciton envelope function squared in reciprocal space. Moreover, under appropriate pump conditions in resonance with exciton excitations, the dispersion at the valence band maximum is renormalized into a camelback-like shape, which has previously been considered as a signature for a driven exciton insulator. We explain both the presence of the satellite band and the renormalization of the highest valence band shape in terms of a self-driven exciton-Floquet phenomenon induced by the photoexcited excitons' time-dependent bosonic field, which leads to a time-dependent single-particle self-energy coupling valence to conduction states—a mechanism similar to one proposed for a phonon- or photon-driven Floquet matter (41, 42) and pump-driven topological phase transitions (43). We demonstrate that, in low dimensional semiconductors, such an exciton-driven Floquet effect can be orders of magnitude larger than the corresponding light-induced Floquet phenomena due to strong electron-hole interactions. Within an effective exciton-Floquet Hamiltonian framework, the results of our ab initio time-dependent adiabatic GW (TD-aGW) calculations are conceptually and quantitatively explained in terms of the dynamics of the pump-induced exciton polarization, which itself plays the role of a driving field.

## Method

Our time-resolved, angle-resolved photoemission spectroscopy simulation in a pump-probe setup is shown in Fig. 1A. For the computed results presented here for monolayer MoS<sub>2</sub>, we use a pump light pulse of the form of a truncated half-period sine squared function in time (*SI Appendix*) with a specific central frequency  $\omega_c$  and a duration of 50 fs. Immediately after the pump, we probe the response with a total measure time of 100 fs. In our TD-aGW method (39), we propagate in time the density matrix  $\rho(t)$  including electron-hole interactions according to

$$i \frac{d\rho(t)}{dt} = [H(t), \rho(t)], \quad [1]$$

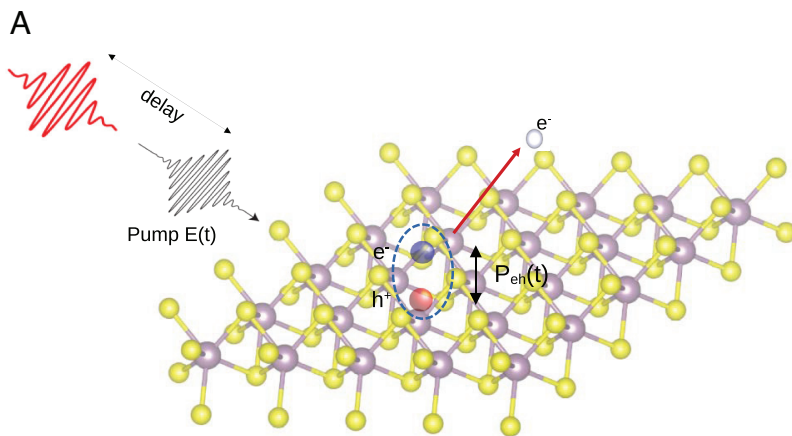


**Fig. 1.** (A) Sketch of the pump-probe setup and the physical picture of exciton polarization induced TR-ARPES signals. (B) Time dependence of the external pump field  $E(t)$ , calculated exciton polarization  $P_{eh}(t)$ , and calculated induced self-energy  $\delta\Sigma(t)$ , for a monolayer MoS<sub>2</sub>.

with

$$H(t) = H^{OP} + \delta V^H(t) + \delta\Sigma^{COHSEX}(t) + U^{ext}(t), \quad [2]$$

where  $H^{OP}$  is the equilibrium GW quasiparticle Hamiltonian,  $\delta V^H$  is the time-dependent change in the Hartree energy term from that of equilibrium,  $\delta\Sigma^{COHSEX}$  is the time-dependent change in self-energy from that of the equilibrium GW self-energy evaluated within the static COHSEX approximation, which describes the electron-hole interaction in the standard static-screening limit, and  $U^{ext}$  is the coupling to the external field (i.e., the pump light). The results for optical response within this formalism in the linear regime of Eq. 1 is equivalent to the solution of the Bethe-Salpeter equation (BSE) with GW quasiparticle states (40, 44, 45). We further assume coherent dynamics without adding dephasing in the simulation. A discussion on the relevant experimental conditions will be given later in the paper. The TR-ARPES spectral intensity from a probe pulse measurement with duration  $T$  is computed from our calculation using the lesser Green function  $G^<$  (46).

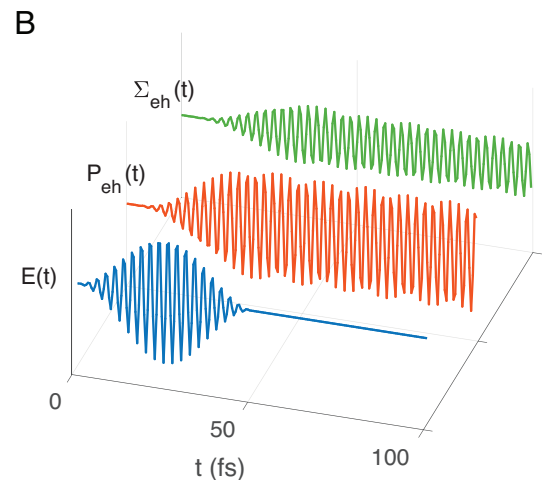
$$I(\omega, T) = -i1/T \int_{T_0}^{T_0+T} dt_1 \int_{T_0}^{T_0+T} dt_2 G^<(t_1, t_2) e^{i\omega(t_2-t_1)}, \quad [3]$$

where  $G^<$  is computed from the density matrix with the  $H(t)$  given in Eq. 2 (47) and the lower limit of the integral  $T_0$  is the starting time of the probe pulse, which is set at the time immediate after the passage of the pump pulse in our simulation. The details of our calculations are given in *SI Appendix*.

We show in Fig. 1B the time profile of a typical light field with pump frequency  $\omega_c$  close to resonance with the energy of an exciton of interest, along with the calculated exciton polarization and the calculated induced self-energy for monolayer MoS<sub>2</sub>. The time dependence of the polarization  $P$  and induced self-energy  $\delta\Sigma$  has a direct consequence on the observed ARPES signals: when the pump frequency is close to the excitation energy of an optically bright exciton, the polarization and the corresponding induced self-energy of the system are large and oscillate at the exciton energy. This oscillations in  $P$  and  $\delta\Sigma$  persist even after the oscillation of the pump pulse decayed, resulting in extended self-energy oscillations that imprint the effects and character of the exciton on the spectral function of the photoexcited hole (i.e., the occupied part of the band structure) and can be observed in ARPES experiments.

## Results

As a demonstration, we evaluate the TR-ARPES for monolayer MoS<sub>2</sub> to take advantage of the large exciton-binding energy and optical strength in atomically thin low-dimensional systems, which is expected to yield more distinct exciton features (48–53). At equilibrium, our GW-BSE calculations (54, 55) performed



using the BerkeleyGW package (56) give an excitation energy for the lowest optically bright “A” exciton of 1.97 eV and a band gap of 2.48 eV. Fig. 2A shows the computed TR-ARPES with a 1.9 eV pump light (in-plane linearly polarized) and a pulse maximum power intensity of  $0.14 \times 10^{10}$  W/cm<sup>2</sup>. The computed valence band dispersion agrees well with the equilibrium band structure (that is, with no pump), which is shown by the blue-dashed lines. Besides the valence band signals, the calculations yield additional features, around the K point, located at 0.50 eV below the conduction band minimum (CBM) or at 1.98 eV above the valence band maximum (VBM). Interestingly, instead of a positive band mass associated with the conduction bands, the extra signal at K has a negative effective band mass, which has been suggested to be an ARPES signature of excitons (21–27). We find that this signal is a satellite feature, replicating the dispersion of the highest valence band around the K point but with a strong  $\mathbf{k}$ -dependent intensity that is largest at the K point, and the energy separation from the VBM (1.98 eV) is virtually identical to the A exciton excitation energy from our direct BSE calculation, indicating that the pump-induced feature is indeed of excitonic origin. To confirm that this feature is originated from electron–hole interaction, we perform a separate simulation with the same setup but without including any electron–hole interactions. The results are shown in Fig. 2B. We clearly see that the extra signal vanishes when the electron–hole interaction is turned off. Moreover, we confirm that the satellite feature is induced by the pump light by comparing with the equilibrium spectral function (SI Appendix).

Since the pump frequency, being 1.9 eV, is off-resonance from the quasiparticle band gap at the K point (which is 2.48 eV), there is negligible conduction band signal. In addition to the ARPES signals from occupied states, we can investigate the unoccupied states (quasi-electron states) by simulating the inverse ARPES. The computed results for inverse ARPES, with and without electron–hole interactions, are shown in Fig. 2C and D, respectively. Similar to the TR-ARPES simulation, we see in the TR-inverse

ARPES intensity a satellite of the conduction band bottom (separated from the conduction band by the exciton excitation energy) in the spectrum that includes electron–hole interactions (Fig. 2C), while there are only signals from the quasi-electron (i.e., conduction) band states in the inverse ARPES spectrum when electron–hole interactions are neglected.

The existence of the valence band satellite feature in the TR-ARPES signals, originating from excitons, and its dispersion can be rationalized in terms of energy conservation: the kinetic energy of the photoemitted electron and the binding energy (measured from the vacuum level) of the hole state left behind in the system must add up to either the photon energy or the photon energy minus an exciton energy (23). Hence, in this simple argument, the dispersion of the extra hole states near the conduction band is the same as that of the equilibrium quasiparticle valence band states. However, this energy argument does not provide any information on the  $\mathbf{k}$ -dependent intensity of the satellite band (which is related to the  $\mathbf{k}$ -space exciton wavefunction) and the argument is only accurate for the dispersion in the weakly pumped regime. Moreover, it cannot predict behaviors corresponding to pump frequency in resonance with the exciton or light intensity in moderately to strongly pumped regimes (Fig. 3 and Fig. 4) that are also readily accessed in contemporary experiments, as we discuss below.

We present here a physical picture for the exciton satellite bands in TR-ARPES by analyzing our ab initio TD-aGW results in terms of an effective Floquet theory. Given the persistent oscillations of the pump-induced self-energy  $\delta\Sigma$  shown in Fig. 1B, to illustrate the physics, we construct a two-band framework for the in-gap excitonic features using the highest valence band and the lowest conduction band. For a pump frequency close to the A exciton energy, a well-defined time-dependent polarization induces a time-dependent coupling between these two quasiparticle bands via  $\delta\Sigma$ , and the oscillation frequency is equal to the A exciton energy. We can write down, after sufficiently time beyond the pump pulse, an effective time-dependent one-particle Hamiltonian,

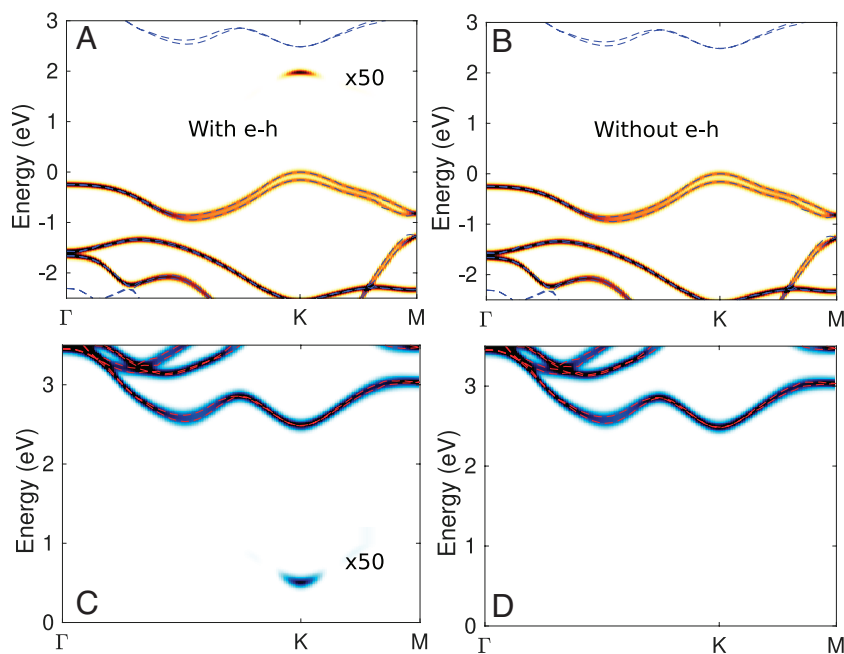


**Fig. 2.** Computed TR-ARPES intensity of monolayer MoS<sub>2</sub>: (A) with electron–hole interaction and (B) without electron–hole interaction with a pump frequency of 1.9 eV of 50-fs duration and a maximum pump power intensity of  $0.14 \times 10^{10}$  W/cm<sup>2</sup>. The spectral intensity near the conduction band is enhanced by 50 times for better visibility. Computed inverse ARPES intensity in a similar pump setup: (C) with e–h interaction and (D) without e–h interaction. The zero of energy is set at the equilibrium valence band maximum.

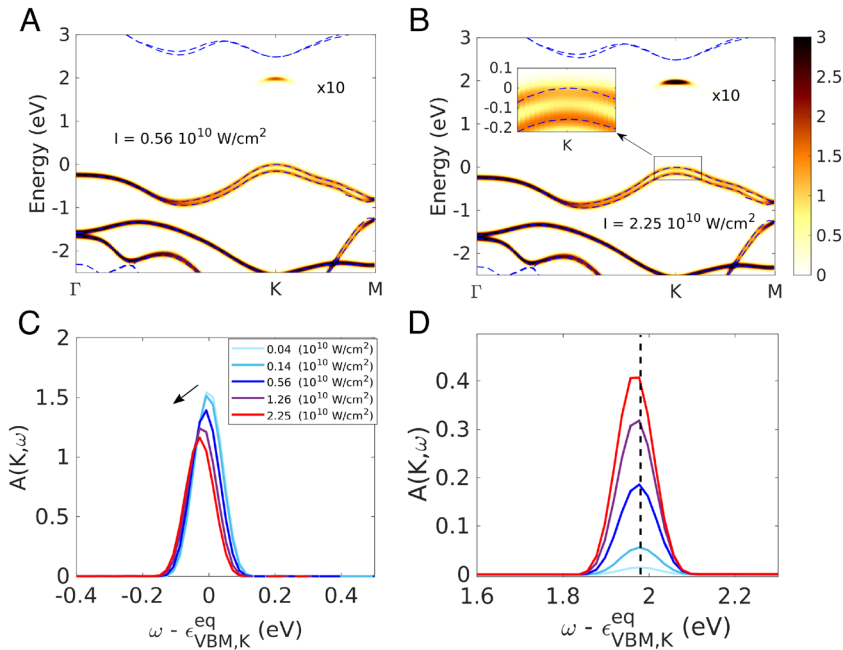


**Fig. 3.** Simulated TR-ARPES with 1.9 eV pump frequency and maximum intensity of (A)  $0.56 \times 10^{10}$  W/cm<sup>2</sup> and (B)  $2.25 \times 10^{10}$  W/cm<sup>2</sup>. *Inset* in (B) shows the quasiparticle band renormalization around the VBM. The spectral intensity above 1 eV is increased by 10 times for visibility. Intensity dependence of spectral function at K for (C) VBM (near 0 eV) and (D) satellite feature (near 2 eV). Black dashed line in (D) indicates the equilibrium A exciton excitation energy from GW-BSE calculation.

$$H^{eff}(t) = \sum_{\mathbf{k}} \begin{pmatrix} \epsilon_{v\mathbf{k}} + \delta\Sigma_{v\mathbf{k}}(t) & \delta\Sigma_{v\mathbf{k}}(t) \\ \delta\Sigma_{c\mathbf{k}}(t) & \epsilon_{c\mathbf{k}} + \delta\Sigma_{c\mathbf{k}}(t) \end{pmatrix}, \quad [4]$$

where  $\epsilon_{v\mathbf{k}}$  and  $\epsilon_{c\mathbf{k}}$  are the quasiparticle energy of states in the valence (hole) and conduction (electron) band with momentum  $\mathbf{k}$ , respectively, and  $\delta\Sigma(t)$  is the polarization-induced time-dependent self-energy, which includes both the change in the Hartree term and in the static COHSEX self-energy in Eq. 2 (SI Appendix). In particular, the off-diagonal term  $\delta\Sigma_{v\mathbf{k}}(t)$  is the self-energy oscillation induced by the exciton coherence. We emphasize that the effective two-band time-dependent Hamiltonian directly emerges from the results from our ab initio calculation: It is directly extracted from our simulation results and not imposed ad hoc into an effective model Hamiltonian. For low pump intensity with a frequency close to an exciton resonance that is optically active, we find  $\delta\Sigma_{c\mathbf{k}}(t) \sim P_{c\mathbf{k}}(t) \sim e^{-iE^X t}$ , where the exciton excitation energy is  $E^X$ ,  $P_{c\mathbf{k}}(t)$  is the time-dependent exciton polarization, and both  $\delta\Sigma_{v\mathbf{k}}$  and  $\delta\Sigma_{c\mathbf{k}}$  are negligible at low pump intensity due to their proportionality to excitation densities. The effective Hamiltonian at each wavevector  $\mathbf{k}$  is formally similar to a two-level system coupled by a periodic field, and there is no coupling between  $\mathbf{k}$ -points owing to an assumed spatially uniform pump field, which is typical experimentally. We note that the time-dependent self-energy operator  $\delta\Sigma(t)$  itself involves a summation over the whole Brillouin zone and its momentum components are related to the envelope function of the exciton (SI Appendix). Solving Eq. 4 within the Floquet formalism, we obtain a discrete series of quasi-energies of exciton-dressed states, which are located at the equilibrium quasiparticle band energy shifted by an integer multiple number of the exciton energy  $E^X$ . The  $\mathbf{k}$ -resolved quasiparticle spectral function of the lesser Green function for a valence band (in our case the highest valence band) that contributes to the ARPES spectrum, within this picture, can be written as (57–59).

$$I_{v\mathbf{k}}(\omega) = \sum_m A_{\mathbf{k}}^m \delta(\omega - E_{v\mathbf{k}} - mE^X), \quad [5]$$

where  $E_{v\mathbf{k}}$  (typically close to  $\epsilon_{v\mathbf{k}}$ ) is the fundamental quasi-energy of the Floquet Hamiltonian,  $m$  is an integer and  $A_{\mathbf{k}}^m$  is an amplitude dictated by the  $\mathbf{k}$ -space exciton envelope function. Since the  $|m| > 1$  terms are from higher order effects, their spectral intensities are

relatively small (57–59) (SI Appendix). From Eq. 5, we can immediately see the origin of the satellite bands: They are Floquet satellite bands of the valence electrons due to a time-dependent oscillating self-energy caused by the presence of excitons.

In addition to the prediction of appearance of multiple self-driven exciton-Floquet (satellite) bands and their  $\mathbf{k}$ -dependent spectral intensity, our calculations in the time domain allows us to account for pump-intensity-dependent features in TR-ARPES spectra. As one increases the pump pulse intensity at near resonant frequency, the satellite intensity becomes larger since the system is driven further away from equilibrium, i.e., higher polarization  $P$ . This is shown in the comparison between Fig. 3 A and B. In addition to the spectral intensity changes, the energy position of the valence band states is shifted at stronger pump intensity. In the *Inset* of Fig. 3B, we see that the photoemission peak position of the VBM is shifted down by 30 meV below its equilibrium energy. This is in contrast to the intensity peaks at wavevectors further away from the K point and that of the next valence band below the VBM, which do not show a shift in energy upon increasing pump intensity. This band-selective renormalization of the main quasiparticle peak is due to the fact that the A exciton of monolayer MoS<sub>2</sub> is mainly consisted of excitations of free electron-hole configurations from the highest valence band. It is also possible to excite (through selection rules and frequency variations) other exciton states with a pump light of narrow bandwidth which may lead to renormalizations of other bands.

The spectral intensity profile near the energy of the VBM at the K point in Fig. 3C summarizes the pump-intensity dependence discussed above. The intensity of the highest valence band signal decreases as we increase the pump intensity, while its peak position shifts to lower energy. At lower intensity, this energy shift in our calculation is linearly proportional to the pump power intensity. On the other hand, the intensity of the satellite signal shown in Fig. 3D increases with pump intensity but the position of its peak in energy only shifts slightly relative to the equilibrium VBM. At weaker pump intensity, the satellite peak position (measured from the equilibrium VBM) agrees with the A exciton excitation energy obtained from our equilibrium GW-BSE calculations as indicated by the black-dashed line.

The amount of valence band renormalization (both in spectral weight and peak position) shows a strong  $\mathbf{k}$ -dependence as seen in Fig. 3B. Such a  $\mathbf{k}$ -dependence can lead to a camel-back feature at

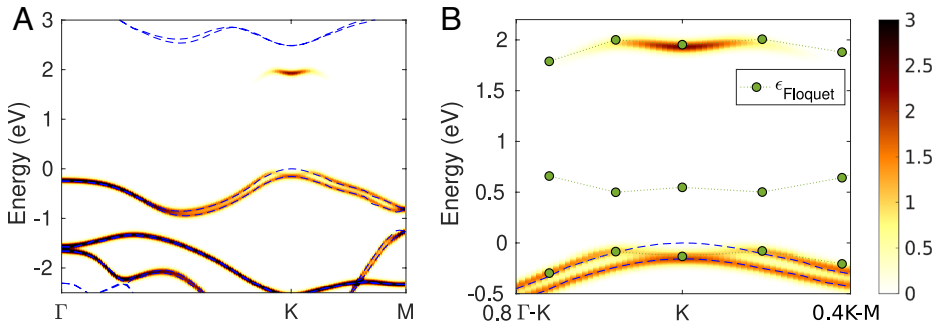


**Fig. 4.** (A) Camel-back features in the simulated TR-ARPES with pump frequency of 2.0 eV and intensity of  $2.25 \times 10^{10}$  W/cm<sup>2</sup>. The spectral intensity above 1 eV is increased by a factor of 2 for visibility. (B) Comparison between the spectral intensity in the region around the VBM from (A) and the quasi-energy bands (green dots) solved from the effective exciton-Floquet Hamiltonian. Blue-dashed lines are the equilibrium bands. The green dots indicate the value of the Floquet quasi-energies only (regardless of their spectral weight), whereas the TR-ARPES results from TD-aGW show both the energy and weight of the spectral function at a given  $\mathbf{k}$  through the color intensity scale. The band of green dots near 0.5 eV is a Floquet  $m = -1$  satellite band associated with the conduction band which should not be visible in TR-ARPES measurements.

higher pump intensity as seen in Fig. 3. In Fig. 4A we show the camel-back dispersion with a pump frequency of 2.0 eV and a pump intensity of  $2.25 \times 10^{10}$  W/cm<sup>2</sup>. Due to the stronger pump intensity and close-to-resonance pump frequency (compared to the results in Fig. 3), the band energy and dispersion as well as spectral weight at the VBM are strongly renormalized while the states at nearby  $\mathbf{k}$  points are less affected. Such a  $\mathbf{k}$ -dependence is caused by the fact that the A exciton has a maximum exciton envelope function amplitude at K (48), and the coupling between interband free electron-hole pairs is strongest for those near this wavevector. At the same time, the dispersion of the satellite band also acquires a camel-back shape, which reflects the corresponding change in the quasiparticle valence band.

The camel-back dispersion can be well reproduced by the effective exciton-Floquet Hamiltonian. In Fig. 4B, we plot the quasi-energy obtained from the Floquet calculations at selected  $\mathbf{k}$  points. We emphasize here that the green dots in Fig. 4B indicate the value of the Floquet quasi-energies only regardless of its spectral weight, whereas the TR-ARPES results from our TD-aGW calculations show both the energy and weight of the spectral function at a given  $\mathbf{k}$  through the color intensity scale. We clearly see that the quasi-energy dispersion agrees well with the TD-aGW spectral intensity peak dispersion of both the highest valence band and its satellite, which validates the physical picture presented above. (The band of green dots near 0.5 eV in Fig. 4B is a Floquet  $m = -1$  satellite band associated with the conduction band which can only be seen in an inverse TR-ARPES measurement.)

Such a camel-back feature has been seen in earlier work (34) and was interpreted as signature of an out-of-equilibrium exciton insulator state created by the optical pump. This out-of-equilibrium exciton insulator proposal originates from an expected camel-back-like renormalization of the VBM and CBM in traditional excitonic insulators, in which the exciton binding energy is comparable to or larger than the quasiparticle bandgap of the normal band insulator phase (15). [This is not true for the present case of a monolayer MoS<sub>2</sub> (48)] Here, we show that camel-back band renormalization in fact arises from a self-driven exciton-Floquet physics, and that this effect can be driven from arbitrary bands and with excitons with either zero or finite center-of-mass (COM) momentum. More generally, excitons generated indirectly through some relaxation process or by means other than light may also lead to such renormalizations, as is the case of spin-dark (i.e., optically inactive owing to spin selection rules) or finite COM-momentum excitons. This is a main difference in the self-driven exciton-Floquet picture with respect to the traditional external light-driven Bloch-Floquet states: In the former, the renormalization only occurs for specific states that couple to the oscillating exciton field; in the latter, replica states emerge throughout the BZ, as long as there are sizeable dipole matrix elements coupling the states to nearby bands.

One can show that in general the band renormalization energy  $\Delta$  obtained from a Floquet mechanism is proportional to the coupling strength squared and inversely proportional to the detuning energy  $\delta$ . A sub-block of a generic Floquet Hamiltonian reads,

$$H^{\text{Floquet}} = \sum_{\mathbf{k}} \begin{pmatrix} \epsilon_{v\mathbf{k}} + \Omega & V_{v\mathbf{k}}(\hbar\omega = \Omega) \\ V_{cv\mathbf{k}}(\hbar\omega = -\Omega) & \epsilon_{c\mathbf{k}} \end{pmatrix}, \quad [6]$$

where  $\Omega$  is the driving frequency and  $V_{v\mathbf{k}}$  is the coupling matrix element. For the light-driven Bloch-Floquet state,  $V_{v\mathbf{k}} \sim d_{v\mathbf{k}}$  and  $\delta = \epsilon_{c\mathbf{k}} - (\epsilon_{v\mathbf{k}} + \Omega)$  so we obtain  $\Delta_{\mathbf{k}}^{\text{light}} \sim \frac{|d_{v\mathbf{k}}|^2}{\delta}$ , where  $d_{v\mathbf{k}}$  is the optical matrix elements, while for exciton-Floquet we have  $V_{v\mathbf{k}} = \delta \Sigma_{v\mathbf{k}}$  and  $\delta = \epsilon_{c\mathbf{k}} - (\epsilon_{v\mathbf{k}} + E_X) = E_b$  so  $\Delta_{\mathbf{k}}^{\text{xct}} \sim \frac{|\delta \Sigma_{v\mathbf{k}}|^2}{E_b} \sim E_b A_{v\mathbf{k}}^2 n_{\text{xct}}$  where  $E_X$  is the exciton excitation energy,  $E_b$  is the exciton binding energy,  $A_{v\mathbf{k}}$  is the exciton envelope function, and  $n_{\text{xct}}$  is the exciton density. We find that, with a photon energy of 2.2 eV and an external field amplitude of  $2 \times 10^{-4}$  a.u., the band renormalization from a light-driven Bloch-Floquet mechanism is about 65 times smaller than that from an exciton-Floquet mechanism in MoS<sub>2</sub>, which makes low-dimensional semiconductors an excellent platform to study Floquet phenomena.

We illustrate the pump-frequency dependence of the band renormalization from ab initio TD-aGW results in Fig. 5A and B. With pump frequency closer to the A exciton resonance at 2.0 eV, the size of the band renormalization grows stronger. We find that energy shift at K is linear to the pump pulse intensity within the intensity range we considered. The valence band renormalization for the hole states can be as large as 100 meV with the strongest pump intensity used here. A similar amount of conduction band renormalization for the electron states is shown in Fig. 5B. This behavior arises from the fact that an on-resonance pumping induces stronger polarization which in turn causes a stronger band renormalization. By analyzing the time snapshot of the Hamiltonian from our TD-aGW results, we find that both the diagonal ( $\delta \Sigma_{vv\mathbf{k}}$ ,  $\delta \Sigma_{cc\mathbf{k}}$ ) and the off-diagonal ( $\delta \Sigma_{vc\mathbf{k}}$ ) self-energy matrix elements in Eq. 4 are of the same order of magnitude under the stronger pump intensity corresponding to Fig. 4B. However, they modify the band gap in opposite directions. The diagonal term shrinks the band gap, while the off-diagonal term leads to a band repulsion. We find that the resulting quasiparticle band gap is increased at both 1.9 eV and 2.0 eV pump frequency considered. However, a dramatic change in band renormalization occurs when the pump frequency is close to the equilibrium interband free electron-hole transition energy, which is at 2.48 eV. At both 2.4 and 2.6 eV pump photon energy, the calculated spectral peak position corresponding to the valence band states instead shifts upward in energy

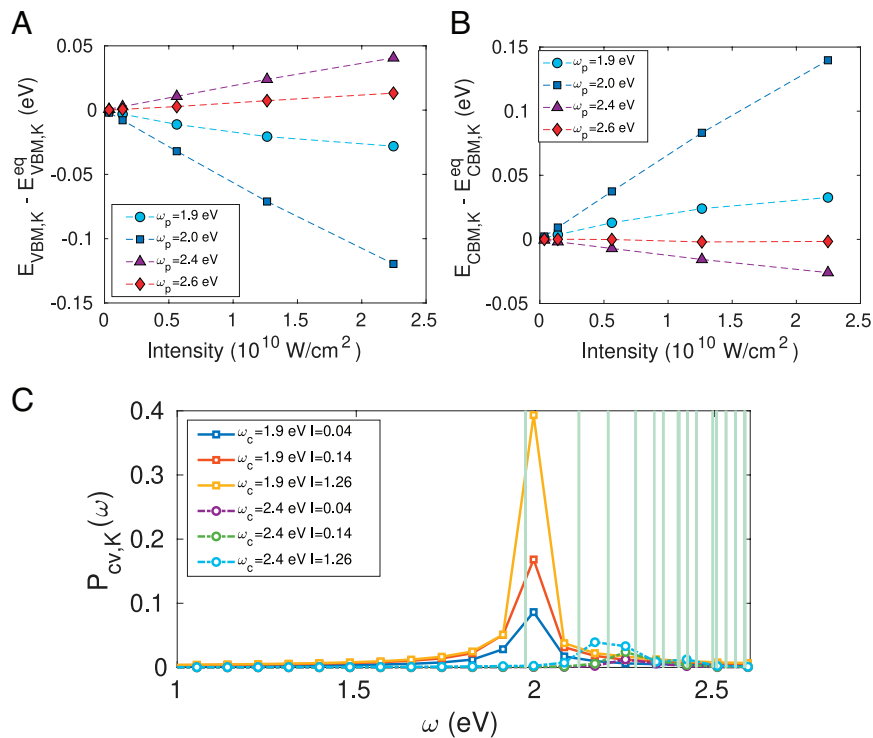


**Fig. 5.** Dependence of (A) the VBM and (B) the CBM energy on pump pulse frequency and intensity. (C) Coherence between the VBM and CBM for several pump pulse frequency and intensity in frequency domain. Light green lines indicate bright exciton excitation energies in this energy window. In panel (C), the intensity is in units of  $10^{10}$  W/cm<sup>2</sup>.

(i.e., lowering the energy for the excited holes). Such opposite band gap correction results from a different physical origin of band renormalization from that of the case with lower pump frequencies that are near resonance with the exciton excitation energy. This happens because, with the pump frequency being close to the electron–hole continuum, the time oscillations of the induced polarization (hence the off-diagonal terms of  $\delta\Sigma_{cv}$ ) at different  $\mathbf{k}$  no longer oscillate at a single frequency, so the overall band repulsion effects are washed out due to the destructive interference of different frequencies of the polarization oscillations. We demonstrate this effect by plotting the coherence between the CBM and the VBM in the frequency domain for several pump settings in Fig. 5C. We can clearly see that the coherent spectrum shows a single strong peak when pumping at 1.9 eV while it shows a much weaker and broader feature when pumping near the continuum. The inherent width associated with the pulse duration (or our simulation time) is 80 meV. Consequently, the band renormalization mainly comes from effects of having an excited carrier density. From our simulations, we see that changes in the carrier density induce changes in the screened exchange energy, which cause an increase in valence band energy and a decrease in the conduction band energy. The magnitude of the band energy shift for this case of pumping with frequency corresponding to the bandgap energy is roughly proportional to the excited carrier density and hence proportional to the light intensity. We also make a distinction between our approach and those traditionally for the optical Stark effect, which address renormalizations of optical transitions due to the presence of an external light field or an exciton population (60, 61). In contrast, our formalism not only describes such results, but also captures a much broader set of microscopic effects such as the renormalization of the quasiparticle band structure, change in the character of the original valence and conduction bands, and emergence of satellite peaks in the quasiparticle spectral function – all of which are naturally understood within the context of Floquet theory.

From the above discussion, we can see that coherent polarizations are crucial to the computationally observed phenomena. We discuss the condition for experiments and justify our simulation setup. First, the ability to excite a single exciton line (thanks to the large exciton binding energy) in atomically thin quasi-2D semiconductors is a significant advance. In contrast, excitons in bulk semiconductors or quantum wells often have a much smaller binding energy, which make it difficult to excite a single exciton level due to the inherent linewidth of the laser pulse. Second, the coherence lifetime in monolayer MoS<sub>2</sub> due to exciton–phonon couplings is about 100 fs at 300 K and can be as long as picoseconds at 100 K (62). The carrier-scattering-limited coherence time was estimated to be 50~150 fs depending on carrier densities (38). Both are of the same order as our simulation length, which justifies our no dephasing assumption. In ref. 26, the instrument temporal resolution is 160~240 fs. Therefore, we expect that the predicted band renormalization can be observed with good sample quality and at low temperature. We note that in a separate work (35) we showed that band renormalization effects can also be observed with fluctuating electron–hole pairs.

In conclusion, we have shown from first-principles time-dependent GW calculations (39) that remarkable excitonic features, containing quantitative information about the exciton energy and wavefunction, can be observed in TR-ARPES experiments with a pump photon energy close to an exciton excitation energy under achievable experimental conditions. We demonstrate that such effects can be significantly stronger than light-induced Floquet effects on monolayer MoS<sub>2</sub>, and, with increasing pump intensity, we observe larger  $\mathbf{k}$ -selective band renormalization (both in energy and dispersion). Our first-principles calculations show that exciton-driven Floquet effects, first theorized in model Hamiltonian calculations (34, 43), are greatly enhanced in low-dimensional materials resulting in a concomitant enhancement of the many-electron

interactions. Our results conclusively demonstrate the signatures of excitons and the quantitative information that may be extracted from them in TR-ARPES experiments, and open an avenue for the accurate study of the properties of excitons, in particular their  $\mathbf{k}$ -space wavefunctions, through careful theoretical and experimental analyses of TR-ARPES.

**Data, Materials, and Software Availability.** All study data are included in the article and/or *SI Appendix*.

**ACKNOWLEDGMENTS.** This work was supported by the Center for Computational Study of Excited State Phenomena in Energy Materials (C2SEPEM), which is funded by the U.S. Department of Energy, Office of Science, Basic Energy Sciences, Materials Sciences and Engineering Division under Contract No. DE-AC02-05CH11231, as part of the Computational Materials Sciences Program. Y.-H.C., D.Y.Q., and F.H.d.J. thank Keshav Dani for

helpful discussion. Y.-H.C. thanks Zhenglun Li and Yi Lin for helpful discussion. We acknowledge the use of computational resources at the National Energy Research Scientific Computing Center (NERSC), a DOE Office of Science User Facility supported by the Office of Science of the U.S. Department of Energy under Contract No. DE-AC02-05CH11231. Y.-H.C. thanks National Center for High-performance Computing (NCHC) for providing computational and storage resources.

Author affiliations: <sup>a</sup>Department of Physics, University of California, Berkeley, CA 94720-7300; <sup>b</sup>Materials Sciences Division, Lawrence Berkeley National Laboratory, Berkeley, CA 94720; <sup>c</sup>Institute of Atomic and Molecular Sciences, Academia Sinica, Taipei 10617, Taiwan; <sup>d</sup>Physics Division, National Center of Theoretical Sciences, Taipei 10617, Taiwan; <sup>e</sup>Department of Mechanical Engineering and Materials Science, Yale University, New Haven, CT 06520; <sup>f</sup>Department of Materials Science and Engineering, Stanford University, Stanford, CA 94305; and <sup>g</sup>Stanford PULSE Institute, Stanford Linear Accelerator Center National Accelerator Laboratory, Menlo Park, CA 94025

1. Y. Y. Peter, M. Cardona, *Fundamentals of Semiconductors, Physics and Materials Properties* (Springer, 2010).
2. H. Haug, S. W. Koch, *Quantum Theory of the Optical and Electronic Properties of Semiconductors* (World Scientific, 1994).
3. T. Mueller, E. Malic, Exciton physics and device application of two-dimensional transition metal dichalcogenide semiconductors. *npj 2D Mater. Appl.* **2**, 29 (2018).
4. G. W. Burg *et al.*, Strongly enhanced tunneling at total charge neutrality in double-bilayer graphene. *Phys. Rev. Lett.* **120**, 177702 (2018).
5. X. Liu, K. Watanabe, T. Taniguchi, B. I. Halperin, P. Kim, Quantum Hall drag of exciton condensate in graphene. *Nat. Phys.* **13**, 746 (2017).
6. J. I. A. Li, T. Taniguchi, K. Watanabe, J. Hone, C. R. Dean, Excitonic superfluid phase in double bilayer graphene. *Nat. Phys.* **13**, 751 (2017).
7. J. Lee *et al.*, Singlet exciton fission photovoltaics. *Acc. Chem. Res.* **46**, 1300–1311 (2013).
8. G. Wang *et al.*, Excitons in atomically thin transition metal dichalcogenides. *Rev. Mod. Phys.* **90**, 021001 (2018).
9. E. J. Sie, C. H. Lui, Y.-H. Lee, J. Kong, N. Gedik, Observation of intervalley biexcitonic optical stark effect in monolayer WS<sub>2</sub>. *Nano Lett.* **16**, 7421 (2016).
10. C.-K. Yong *et al.*, Biexcitonic optical Stark effects in monolayer molybdenum diselenide. *Nat. Phys.* **14**, 1092 (2018).
11. P. Narang, C. A. C. Garcia, C. Felser, The topology of electronic band structures. *Nat. Mater.* **20**, 293–300 (2021).
12. A. de la Torre *et al.*, Nonthermal pathways to ultrafast control in quantum materials. *Rev. Mod. Phys.* **93**, 041002 (2021).
13. F. Schmitt *et al.*, Transient electronic structure and melting of a charge density wave in TbTe<sub>3</sub>. *Science* **321**, 1649 (2008), <https://science.sciencemag.org/content/321/5896/1649.full.pdf>.
14. T. Rohwer *et al.*, Collapse of long-range charge order tracked by time-resolved photoemission at high momenta. *Nature* **471**, 490 (2011).
15. S. Mor *et al.*, Ultrafast electronic band gap control in an excitonic insulator. *Phys. Rev. Lett.* **119**, 086401 (2017).
16. F. Liu, M. E. Ziffer, K. R. Hansen, J. Wang, X. Zhu, Direct determination of band-gap renormalization in the photoexcited monolayer MoS<sub>2</sub>. *Phys. Rev. Lett.* **122**, 246803 (2019).
17. R. Bertoni *et al.*, Generation and evolution of spin-, valley-, and layer-polarized excited carriers in inversion-symmetric WSe<sub>2</sub>. *Phys. Rev. Lett.* **117**, 277201 (2016).
18. S. Ulstrup *et al.*, Ultrafast band structure control of a two-dimensional heterostructure. *ACS Nano* **10**, 6315 (2016).
19. F. Andreata *et al.*, Transient hot electron dynamics in single-layer TaS<sub>2</sub>. *Phys. Rev. B* **99**, 165421 (2019).
20. R.-Y. Liu *et al.*, Symmetry-breaking and spin-blockage effects on carrier dynamics in single-layer tungsten diselenide. *Phys. Rev. B* **100**, 214309 (2019).
21. J. H. Buss *et al.*, A setup for extreme-ultraviolet ultrafast angle-resolved photoelectron spectroscopy at 50-kHz repetition rate. *Rev. Sci. Instrum.* **90**, 023105 (2019), [10.1063/1.5079677](https://doi.org/10.1063/1.5079677).
22. A. Steinhoff *et al.*, Exciton fission in monolayer transition metal dichalcogenide semiconductors. *Nat. Commun.* **8**, 1166 (2017).
23. A. Rustagi, A. F. Kemper, Photoemission signature of excitons. *Phys. Rev. B* **97**, 235310 (2018).
24. H. Ohnishi *et al.*, Direct determination of exciton wavefunction amplitudes by the momentum-resolved photo-electron emission experiment. *Int. J. Mod. Phys. B* **32**, 1850094 (2018).
25. E. Perfetto, D. Sangalli, A. Marini, G. Stefanucci, First-principles approach to excitons in time-resolved and angle-resolved photoemission spectra. *Phys. Rev. B* **94**, 245303 (2016).
26. J. Madéo *et al.*, Directly visualizing the momentum-forbidden dark excitons and their dynamics in atomically thin semiconductors. *Science* **4**, 1199 (2020).
27. M. K. L. Man *et al.*, Experimental measurement of the intrinsic excitonic wave function. *Sci. Adv.* **7**, eabg0192 (2021).
28. S. Dong *et al.*, Direct measurement of key exciton properties: Energy, dynamics and spatial distribution of the wave function. *Nat. Sci.* **1**, e10010 (2021).
29. R. Wallauer *et al.*, Momentum-resolved observation of exciton formation dynamics in monolayer WS<sub>2</sub>. *Nano Lett.* **21**, 5867–5873 (2021).
30. O. Karni *et al.*, Moiré-localized interlayer exciton wavefunctions captured by imaging its electron and hole constituents. *arXiv [Preprint]* (2021), <https://doi.org/10.48550/arXiv.2108.01933> (Accessed 8 April 2021).
31. D. Christensen, M. Selig, E. Malic, R. Ernstorfer, A. Knorr, Theory of exciton dynamics in time-resolved ARPES: Intra- and intervalley scattering in two-dimensional semiconductors. *Phys. Rev. B* **100**, 205401 (2019).
32. N. H. Kwong, G. Rupper, R. Binder, Self-consistent T-matrix theory of semiconductor light-absorption and luminescence. *Phys. Rev. B* **79**, 15 (2009).
33. T. Yoshioka, K. Asano, Classical-quantum crossovers in quasi-one-dimensional electron-hole systems: Exciton-Mott physics and interband optical spectra. *Phys. Rev. B* **86**, 115314 (2012).
34. E. Perfetto, D. Sangalli, A. Marini, G. Stefanucci, Pump-driven normal-to-excitonic insulator transition: Josephson oscillations and signatures of BEC-BCS crossover in time-resolved ARPES. *Phys. Rev. Mater.* **3**, 124601 (2019).
35. Y. Lin *et al.*, Exciton-driven renormalization of quasiparticle band structure in monolayer MoS<sub>2</sub>. *Phys. Rev. B* **106**, L081117 (2022).
36. E. Perfetto, S. Bianchi, G. Stefanucci, Time-resolved ARPES spectra of nonequilibrium excitonic insulators: Revealing macroscopic coherence with ultrashort pulses. *Phys. Rev. B* **101**, 041201 (2020).
37. D. Sangalli, Excitons and carriers in transient absorption and time-resolved ARPES spectroscopy: An ab initio approach. *Phys. Rev. Mater.* **5**, 083803 (2021).
38. E. Perfetto, Y. Pavlyukh, G. Stefanucci, Real-time GW: Toward an ab initio description of the ultrafast carrier and exciton dynamics in two-dimensional materials. *Phys. Rev. Lett.* **128**, 016801 (2022).
39. Y. H. Chan, D. Y. Qiu, F. H. da Jornada, S. G. Louie, Giant exciton-enhanced shift currents and direct current conduction with subbandgap photo excitations produced by many-electron interactions. *Proc. Natl. Acad. Sci. U.S.A.* **118**, e1906938118 (2021).
40. C. Attaccalite, M. Grüning, A. Marini, Real-time approach to the optical properties of solids and nanostructures: Time-dependent Bethe-Salpeter equation. *Phys. Rev. B* **84**, 245110 (2011).
41. H. Hübener, U. De Giovannini, A. Rubio, Phonon driven Floquet matter. *Nano Lett.* **18**, 1535–1542 (2018).
42. U. De Giovannini, H. Hübener, A. Rubio, Monitoring electron-photon dressing in WSe<sub>2</sub>. *Nano Lett.* **16**, 7933–7998 (2016).
43. E. Perfetto, G. Stefanucci, Floquet topological phase of Nondriven *p*-wave nonequilibrium excitonic insulators. *Phys. Rev. Lett.* **125**, 106401 (2020).
44. D. Rocca, D. Lu, G. Galli, Ab initio calculations of optical absorption spectra: Solution of the Bethe-Salpeter equation within density matrix perturbation theory. *J. Chem. Phys.* **133**, 164109 (2010).
45. E. Rabani, R. Baer, D. Neuhauser, Time-dependent stochastic Bethe-Salpeter approach. *Phys. Rev. B* **91**, 235302 (2015).
46. J. K. Freericks, H. R. Krishnamurthy, T. Pruschke, Theoretical description of time-resolved photoemission spectroscopy: Application to pump-probe experiments. *Phys. Rev. Lett.* **102**, 136401 (2009).
47. G. Stefanucci, R. van Leeuwen, *Nonequilibrium Many-Body Theory of Quantum Systems: A Modern Introduction*, 1sted (Cambridge University Press, 2013).
48. D. Y. Qiu, F. H. da Jornada, S. G. Louie, Optical spectrum of MoS<sub>2</sub>: Many-body effects and diversity of exciton states. *Phys. Rev. Lett.* **111**, 216805 (2013). Erratum: *Phys. Rev. Lett.* **115**, 119901 (2015).
49. D. Y. Qiu, F. H. da Jornada, S. G. Louie, Screening and many-body effects in two-dimensional crystals: Monolayer MoS<sub>2</sub>. *Phys. Rev. B* **93**, 235435 (2016).
50. A. Chernikov *et al.*, Exciton binding energy and nonhydrogenic rydberg series in monolayer WS<sub>2</sub>. *Phys. Rev. Lett.* **113**, 076802 (2014).
51. M. M. Ugeda *et al.*, Giant bandgap renormalization and excitonic effects in a monolayer transition metal dichalcogenide semiconductor. *Nat. Mater.* **13**, 1091–1095 (2014).
52. B. Zhu, X. Chen, X. Cui, Exciton binding energy of monolayer WS<sub>2</sub>. *Sci. Rep.* **5**, 9218 (2015).
53. Z. Ye *et al.*, Probing excitonic dark states in single-layer tungsten disulphide. *Nature* **513**, 214–218 (2014).
54. M. S. Hybertsen, S. G. Louie, Electron correlation in semiconductors and insulators: Band gaps and quasiparticle energies. *Phys. Rev. B* **34**, 5390 (1986).
55. M. Rohlfing, S. G. Louie, Electron-hole excitations and optical spectra from first principles. *Phys. Rev. B* **62**, 4927 (2000).
56. J. Deslippe *et al.*, BerkeleyGW: A massively parallel computer package for the calculation of the quasiparticle and optical properties of materials and nanostructures. *Comput. Phys. Commun.* **183**, 1269 (2012).
57. B. M. Fregoso, Y. H. Wang, N. Gedik, V. Galitski, Driven electronic states at the surface of a topological insulator. *Phys. Rev. B* **88**, 155129 (2013).
58. H. Deghani, A. Mitra, Optical hall conductivity of a Floquet topological insulator. *Phys. Rev. B* **92**, 165111 (2015).
59. Q. Chen, L. Du, G. A. Fiete, Floquet band structure of a semi-Dirac system. *Phys. Rev. B* **97**, 035422 (2018).
60. E. Sie *et al.*, Valley-selective optical Stark effect in monolayer WS<sub>2</sub>. *Nat. Mater.* **14**, 290–294 (2015), [10.1038/nmat4156](https://doi.org/10.1038/nmat4156).
61. C. K. Yong *et al.*, Biexcitonic optical Stark effects in monolayer molybdenum diselenide. *Nat. Phys.* **14**, 1092–1096 (2018), [10.1038/s41567-018-0216-7](https://doi.org/10.1038/s41567-018-0216-7).
62. Y. H. Chan *et al.*, Exciton lifetime and optical linewidth profile via exciton-phonon interactions: Theory and first-principles calculations for monolayer MoS<sub>2</sub>. *Nano Lett.* **23**, 3971–3977 (2023), [10.1021/acs.nanolett.3c00732](https://doi.org/10.1021/acs.nanolett.3c00732).